OPEN ACCESS



Interplanetary Type IV Solar Radio Bursts: A Comprehensive Catalog and Statistical Results

Atul Mohan^{1,2}, Nat Gopalswamy¹, Anshu Kumari¹, Sachiko Akiyama^{1,2}, and Sindhuja G^{1,2,3}, has A Goddard Space Flight Center, Greenbelt, MD 20771, USA; atul.mohan@nasa.gov

² The Catholic University of America, Washington, DC 20064, USA

³ Bangalore University, Mysore Rd, Jnana Bharathi, Bengaluru, Karnataka, India

*Received 2024 April 15; revised 2024 May 20; accepted 2024 May 31; published 2024 August 7

Abstract

Decameter hectometric (DH; 1-14 MHz) type IV radio bursts are produced by flare-accelerated electrons trapped in postflare loops or the moving magnetic structures associated with the coronal mass ejections (CMEs). From a space weather perspective, it is important to systematically compile these bursts, explore their spectrotemporal characteristics, and study the associated CMEs. We present a comprehensive catalog of DH type IV bursts observed by the Radio and Plasma Wave Investigation instruments on board the Wind and Solar TErrestrial RElations Observatory spacecraft covering the period of white-light CME observations by the Large Angle and Spectrometric Coronagraph on board the Solar and Heliospheric Observatory mission between 1996 November and 2023 May. The catalog has 139 bursts, of which 73% are associated with a fast (>900 km s⁻¹) and wide (>60°) CME, with a mean CME speed of 1301 km s⁻¹. All DH type IV bursts are white-light CME-associated, with 78% of the events associated with halo CMEs. The CME source latitudes are within ±45°. Seventy-seven events had multiple-vantage-point observations from different spacecraft, letting us explore the impact of the line of sight on the dynamic spectra. For 48 of the 77 events, there were good data from at least two spacecraft. We find that, unless occulted by nearby plasma structures, a type IV burst is best viewed when observed within a $\pm 60^{\circ}$ line of sight. Also, bursts with a duration above 120 minutes have source longitudes within $\pm 60^{\circ}$. Our inferences confirm the inherent directivity in the type IV emission. Additionally, the catalog forms a Sun-as-a-star DH type IV burst database.

Unified Astronomy Thesaurus concepts: Active Sun (18); Solar radio flares (1342); Solar coronal mass ejections (310); Stellar coronal mass ejections (1881); Space weather (2037); Catalogs (205)

1. Introduction

Type IV radio bursts were first classified in the meter wave band by Boischot (1957). They appear as broadband continuum features in the dynamic spectrum and come in two flavors: stationary type IV and moving type IV (Takakura & Kai 1961; Young et al. 1961; Kundu & Spencer 1963). A moving type IV burst shows a clear drift in the dynamic spectrum, while the stationary type IV bursts do not. The sources of moving type IV bursts were soon recognized to be moving away from the Sun (Weiss 1963; Boischot & Clavelier 1968). Using simultaneous white-light and radio (80 MHz) observations of the K corona, Hansen et al. (1971) demonstrated that moving type IV bursts are associated with bright coronal transients and derived a speed of 1300 km s⁻¹. Moving type IV bursts were soon recognized as being produced by flare-accelerated electrons trapped in moving magnetized plasmoids associated with coronal mass ejections (CMEs; e.g., Takakura 1961; Kundu & Spencer 1963; Dulk & Altschuler 1971; Smerd 1971; Schmahl 1972). Robinson (1978) performed a statistical analysis of 23 moving type IV bursts observed by the Culgoora radioheliograph and estimated the source speeds to lie within 200–1500 km s⁻¹. Meanwhile, the stationary type IVs are produced by accelerated electrons trapped in postflare loops (see Wild 1970; McLean & Labrum 1985 for an overview). The emission mechanism of the type IV bursts is

Original content from this work may be used under the terms of the Creative Commons Attribution 4.0 licence. Any further distribution of this work must maintain attribution to the author(s) and the title of the work, journal citation and DOI.

believed to be primarily via a plasma emission process based on observed polarization and brightness temperature levels (e.g., Weiss 1963; Duncan 1981; Gopalswamy & Kundu 1989). Using 15 yr of metric burst data from the Culgoora radioheliograph, Cane & Reames (1988a) showed that ∼88% of the 227 metric type IV bursts were associated with a type II burst, which is produced by electrons accelerated by CME shocks (e.g., Smerd 1970; Wild 1970; Gopalswamy et al. 2005; Kumari et al. 2023). However, only around a third of the type II bursts had a type IV link. Type IVs are closely connected to strong soft X-ray flares (on average with M-class flares), especially ones that last for around 1 hr or longer, and fast CMEs (Cane & Reames 1988b). Similarly, around 81% of the type IVs in cycle 24 were found to be associated with whitelight CMEs (Kumari et al. 2021). However, some of their cases of nonassociations could be influenced by data gaps or stealth CMEs (e.g., Robbrecht et al. 2009; D'Huys et al. 2014; Morosan et al. 2021), which are known to have no white-light signatures. In such a case, the percentage of association can

Decameter hectometric (DH) type IV bursts are rare continuations of the metric type IVs into interplanetary space and are almost always associated with fast (>900 km s⁻¹) and wide (>60° angular extent) CMEs and thereby with solar energetic particle events (SEPs; Gopalswamy 2004b, 2011; Hillaris et al. 2016). Unlike the metric type IVs, DH type IVs are always associated with CMEs that have a mean speed ($V_{\rm mean}$) of ~1500 km s⁻¹ and are ~75% of the time halo CMEs (Gopalswamy 2011). About 89% of these bursts are associated with GOES M- and X-class flares (Hillaris et al. 2016).

Exploring the CMEs between 1996 and 2006 that caused an SEP and a radio burst in the decimeter to kilometer band, Miteva et al. (2017) showed that the median X-ray flare strength and CME speed are the highest for the events associated with DHkilometer type IV bursts. DH type IVs are observed below 14 MHz and occasionally extend down to 1 MHz with a mean extent down to \sim 7 MHz (Gopalswamy 2011). They last for \sim 1 hr, occasionally extending over days (Hillaris et al. 2016). Since emission at frequencies below ~10 MHz cannot to be observed from the ground due to the ionospheric cutoff, these events can be detected only with space-based instruments (Gopalswamy 2011). The Radio and Plasma Wave Investigation (WAVES; Bougeret et al. 1995) instrument on board the Wind spacecraft and the SWAVES instrument on board the Solar TErrestrial RElations Observatory (STEREO; Howard et al. 2008) spacecraft are the only windows into this interplanetary radio emission. Despite the close association of DH type IV bursts with SEPs, strong X-ray flares, and fast and wide CMEs, there have been only a few studies of DH type IV events compared to other types of solar radio bursts. This is primarily because these events are relatively rare (Hillaris et al. 2016), making it difficult to obtain a significant sample to explore their statistical behavior in a robust manner. The results mentioned above on the DH type IV bursts had only ~40 events, mainly from just one solar cycle (C23) and primarily from the Wind spacecraft. Besides, Gopalswamy et al. (2016) reported that the DH type IV emission was directed within a cone angle of $\pm 60^{\circ}$, which is possibly associated with the line-of-sight occultation of the postflare loop by the solar disk. Using a few case studies with multiple-vantage-point data from the Wind and STEREO missions, Talebpour Sheshvan & Pohjolainen (2018) argued that the visibility of the DH type IV could be hampered by the presence of high-density structures along the line of sight that are formed by the interaction of the evolving CME with other preexisting coronal magnetic field structures like streamers. These high-density regions can attenuate the DH-band radio emission from the postflare loop. However, to make robust conclusions on various characteristics of DH type IVs and the properties of the CMEs/flares that correlate with the observed burst features, we need a statistically complete and significant sample.

In this work, we aim to put together a comprehensive sample of DH type IV bursts detected by the Wind and STEREO spacecraft and catalog the properties of the associated CMEs. The catalog covers two full solar cycles (C23 and C24) and the start of the current cycle (C25), providing a statistically significant sample for exploration. The DH-band spectrotemporal properties of these bursts will be explored alongside the properties of their associated CMEs. We will also address the issue of directivity in the events detected simultaneously by at least two widely separated spacecraft. Recently, Patel et al. (2021) studied DH type II radio bursts during the past two solar cycles. Since type IVs and type IIs are generally considered as a radio diagnostic of strong CMEs, this work will complement the aforementioned study, forming a unique combined database of particle acceleration signatures of interplanetary CMEs. Besides, type IV radio bursts are the only solar-type bursts to be reported so far on other active stars (Zic et al. 2020; Mohan et al. 2024). Since our observations are full solar-disk-integrated emission, this database will form the first comprehensive Sun-as-a-star catalog of interplanetary type IV bursts.

Section 2 presents the sources of data, while Section 3 describes the steps involved in identifying and compiling the

DH type IV events from the data sources. Section 4 presents the DH type IV catalog and the statistical properties of these events. Section 5 analyzes the results and discusses their implications. The conclusions are given in Section 6.

2. Data

The data primarily come from the compilation of the Coordinated Data Analysis Workshops (CDAW) Data Center.⁴ This work made use of the radio dynamic spectra (DS) from the Wind, STEREO-A, and STEREO-B spacecraft in the frequency range 0.02-14 MHz. The properties of the whitelight CMEs observed by the Large Angle and Spectrometric COronagraph (LASCO; Brueckner et al. 1995) on board the Solar and Heliospheric Observatory⁵ are obtained from the LASCO CME catalog (Yashiro et al. 2004; Gopalswamy et al. 2009). We relied on the event reports from the Space Weather Prediction Center⁶ (SWPC) to obtain the list of metric type IV events since 1996. Besides, in some cases, we relied on various other public data sources to identify metric counterparts of DH type IVs, namely e-Callisto, Radio Monitoring, and the Australian Space Weather Database. The DH type II catalog (Gopalswamy et al. 2019) compiled by the CDAW Data Center is also used, since they are often associated with type IVs and CMEs.

3. Methodology

We adopt a strategy of bias-free blind search for DH type IV burst signatures. Since DH type IV bursts are very closely associated with CMEs, the initial list of potential date-time periods to search for DH type IV bursts was provided by the LASCO CME catalog. However, we may still miss some DH type IV events due to potential data gaps in the LASCO data stream or events not being associated with white-light CMEs. To cover such periods and ensure sample completeness, we relied on two other catalogs of bursts potentially associated with DH type IV bursts: metric type IV event reports and the DH type II catalog. Since DH type IVs are continuations of metric type IVs, the date-time periods from SWPC metric type IV reports should provide a larger set of potential DH type IV events. Nevertheless, the reason why we did not solely rely on the SWPC metric type IV reports to search for DH type IVs is that there have been cases where radio bursts go unreported in the SWPC event list. The DH type II catalog, being an independent DH-band catalog of CME-associated radio bursts, also provides additional date-time intervals, helping us cover the period of the LASCO data gap. The date-time interval we chose for the study extends from 1996 November to 2023 May, which is when LASCO data started being available. This ensures that we have a well-defined, systematically compiled catalog of CME characteristics covering multiple solar cycles (Yashiro et al. 2004; Gopalswamy et al. 2009). The final list of DH type IV search periods includes date-times corresponding to 34,083 LASCO CMEs, 939 metric type IVs, and 140 DH type IIs.

⁴ https://cdaw.gsfc.nasa.gov/

https://www.eoportal.org/satellite-missions/soho

https://www.swpc.noaa.gov/products/solar-and-geophysical-event-reports

https://www.e-callisto.org/links.html

https://secchirh.obspm.fr/spip.php?rubrique8

https://www.sws.bom.gov.au/World_Data_Centre/1/1

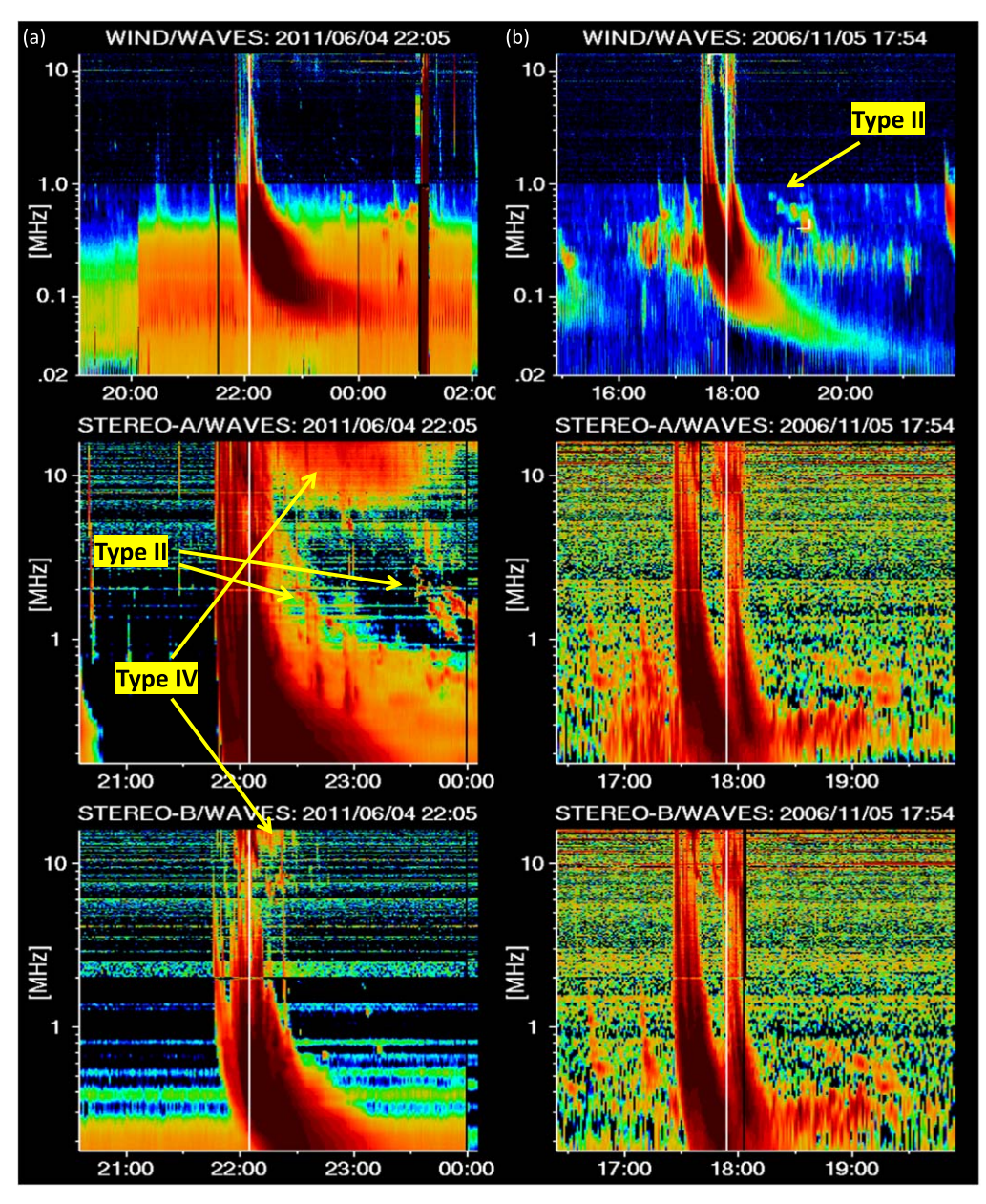


Figure 1. Example DH DS. (a) A type IV detection in STEREO-A and B. (b) No type IV burst, but a type II is detected by multiple spacecraft. The time periods of the associated LASCO CME events are marked by vertical white lines.

A Python code was written to gather the DS from Wind and STEREO for each date—time entry in the search list by querying the respective databases. ^{10,11} Whenever there are data from multiple missions, a combined DS is made. All the images were manually examined later to identify DH type IV candidates. Figure 1 shows example DH DS from periods with and without a type IV event. After identifying the DH type IV candidates, the metric DS were also accumulated for all events and ensured that there is a potential continuation of the DH type IV into the metric band. We removed a couple of very long-duration type IV bursts extending over 10 hr because of the difficulty in associating them with a particular CME event. These events can cause ambiguity in the scientific inferences derived on the relationship between DH type IV characteristics, particularly the duration and properties of associated CMEs. Thus, we ended

up with a preliminary sample of DH type IV events, each of which is well associated with a CME. The preliminary DH type IV sample was compared against existing event lists used by previous studies (Gopalswamy 2011; Gopalswamy et al. 2016; Hillaris et al. 2016) to ensure completeness across them. It was also ensured that the metric DS, whenever available, from a ground-based data repository had signatures of type IV counterparts. Some spurious candidates with no clear metric counterparts were thus removed from the DH type IV catalog.

4. Results

The final DH type IV sample contains 139 events, each of which is well associated with a white-light CME. This is in contrast to the case of metric type IV bursts, which can occur without an associated white-light CME (Kumari et al. 2021). The sample has more events than previously reported for the specific periods covered by previous works. For instance, in the

https://cdaw.gsfc.nasa.gov/images/wind/

¹¹ https://cdaw.gsfc.nasa.gov/images/stereo/

(a) DH type-IV catalog

Type-IV properties							Type IV source view							Quality metrics		CME				Other info		
Date	Time	Dur (min)	End Freq (MHz)	M/S	Wind M/S	STA M/S	STB M/S	Best view spacecraft	Spacecraft	STB-Earth Angle (deg)	STA-Earth Angle (deg)	Src in Wind FoV (deg)	Src in STA FoV (deg)	Src in STB FoV (deg)	Event Quality	Data Quality	Date	Time	Flare loc	V_mean (km/s)	Solar Cycle	DH typell event
2023/04/21	18:24	36	9.7	S	S	S	NA	Wind	Wind;STA	5.9	-10.3	11	21.3	5.2	S212	W2A1B0	2023/04/21	18:12:06	S22W11	1284	25	Y
2023/03/06	11:04	59	12.6	S	S	NA	NA	Wind	Wind	7.6	-12.5	nan	nan	nan	S1I1	W2A2B0	2023/03/06	10:48:05	BL239	479	25	Y
2023/01/11	01:25	67	12.3	S	S	S	NA	Wind	Wind;STA	8.3	-13.6	-67	-53.4	-75.3	S2I1	W2A1B0	2023/01/11	01:25:53	N25E66	1083	25	N
2022/08/28	16:21	110	6.4	M	M	M	NA	Wind	Wind;STA	15.1	-20.1	85	105.1	69.9	S3I3	W2A2B0	2022/08/28	16:12:05	S30W85	1232	25	Y
2022/08/27	02:30	56	11	S	S	S	NA	STA	Wind;STA	15.3	-20.3	58	78.3	42.8	S213	W2A1B0	2022/08/27	02:24:06	S19W58	1284	25	Y
2022/08/18	11:15	28	11	М	M	M	NA	Wind	Wind;STA	16.2	-21.2	37	58.2	20.8	S112	W2A2B0	2022/08/18	11:00:05	S27W37	1327	25	Y
2022/07/08	21:25	62	9.2	S	S	NA	NA	Wind	Wind	20	-24.9	-40	-15.1	-60	S2I3	W2A1B0	2022/07/08	20:36:05	N20E40	1223	25	Υ
2022/03/30	18:00	46	12.2	S	S	NA	NA	Wind	Wind	29.1	-32.9	31	63.9	1.9	S213	W2A1B0	2022/03/30	18:00:05	N13W31	641	25	N
2022/01/29	23:35	207	10	S	S	S	NA	STA	Wind;STA	31.9	-34.7	-6	28.7	-37.9	S213	W2A2B0	2022/01/29	23:36:06	N18E06	530	25	N
2017/09/17	12:05	55	7.9	М	NA	M	NA	STA	STA	128.6	-127.6	-170	-42.4	61.4	S3I3	W2A2B0	2017/09/17	12:00:06	S08E170	1385	24	Y
2017/09/16	11:55	256	3.4	S	NA	S	NA	STA	STA	128.6	-127.7	177	-55.3	48.4	S3I3	W2A0B0	2017/09/16	12:12:05	S04W177	325	24	N
2016/04/18	00:55	58	4.2	M	М	М	NA	STA	STA;Wind	152	-160.7	nan	nan	nan	S3I3	W2A2B0	2016/04/18	00:48:04		1084	24	N
2016/02/21	12:00	100	9.9	S	NA	S	NA	STA	STA	159.2	-163.7	155	-41.3	-4.2	S3I1	W2A2B0	2016/02/21	12:00:04	N08W155	533	24	N
2015/11/04	14:14	27	5.9	M	M	NA	NA	Wind	Wind	174.4	-168.3	4	172.3	-170.4	S213	W2A0B0	2015/11/04	14:48:04	N09W04	578	24	Y

(b) Properties of CMEs associated with DH type-IV bursts

					Width	V_mean	V_fin	V_20R	accel			MPA		
Date	DHtypeIV time	CME Time	Flare	PA (deg)	(deg)	(km/s)	(km/s)	(km/s)	(m/s ²)	M (g)	KE (erg)	(deg)	Spacecraft	Remarks
2023/04/21	18:24	18:12:06	M1.7	Halo	360	1284	1100	1216	-28.1	nan	nan	180	Wind;STA	None
2023/03/06	11:04	10:48:05		233	45	479	554	576	7.2	nan	nan	229	Wind	None
2023/01/11	01:25	01:25:53	M2.4	67	89	1083	1033	1063	-6.7	nan	nan	72	Wind;STA	None
2022/08/28	16:21	16:12:05	M6.7	Halo	360	1232	1088	1168	-21.2	nan	nan	243	Wind;STA	None
2022/08/27	02:30	02:24:06	M4.8	Halo	360	1284	1198	1261	-12.1	nan	nan	225	Wind;STA	None
2022/08/18	11:15	11:00:05	M1.5	Halo	360	1327	1164	1216	-28.9	nan	nan	174	Wind;STA	None
2022/07/08	21:25	20:36:05	M2.5	Halo	360	1223	1051	1181	-23.3	nan	nan	77	Wind	None
2022/03/30	<u>18:00</u>	18:00:05	X1.3	Halo	360	641	573	531	-9.3	nan	nan	298	Wind	None; accel*1
2022/01/29	23:35	23:36:06	M1.1	Halo	360	530	434	379	-10.1	nan	nan	58	Wind;STA	None
2017/09/17	12:05	12:00:06		Halo	360	1385	1187	1308	-32.8	1.50E+16	1.50E+32	72	STA	None; M*2; KE*2
2017/09/16	<u>11:55</u>	12:12:05		112	8	325	272	51	-6.1	nan	nan	112	STA	Poor Event; accel*1
2016/04/18	00:55	00:48:04		275	162	1084	895	1041	-24.6	1.10E+16	6.30E+31	291	STA;Wind	Partial Halo; M*2; KE*2
2016/02/21	12:00	12:00:04		Halo	360	533	517	510	-1.7	3.60E+15	5.10E+30	298	STA	None; accel*1; M*2; KE*2
2015/11/04	14:14	14:48:04	M3.7	Halo	360	578	650	701	10.1	6.60E+15	1.10E+31	288	Wind	None; accel*1; M*2; KE*2

Figure 2. (a) A portion of the DH type IV catalog. (b) The corresponding table of properties of the associated CMEs.

period 1998–2012, we report 91 events, as opposed to the 48 reported by Hillaris et al. (2016). The rise in source count is partly because of the addition of data from the STEREO spacecraft, unused in Hillaris et al. (2016). But, even if only the Wind/WAVES data within 1998-2012 are considered, our catalog has 71 events with a type IV signature. Similarly, the current list has 65 Wind/WAVES events in cycle 23, compared to the 42 events reported by Gopalswamy (2011). This rise in the source count can be attributed to the blind search strategy employed by combining date-time periods across the metric type IV list, the DH type II catalog, and the LASCO CME catalog. Also, the addition of STEREO data helped confirm some faint type IVs in the Wind/WAVES data that would have been omitted previously. Such faint events could then be confirmed based on the detection of metric type IV counterparts from ground-based data.

Now that the authenticity of events in our sample and completeness across earlier catalogs are verified, we put together a catalog of the characteristics of these bursts in the radio DS, the properties of the associated CMEs, and the flare location as recorded by multiple spacecraft. The latter gives a range of viewing angles for each event, letting one explore the directivity of type IV bursts. The following subsection describes the contents of the catalog.

4.1. The DH Type IV Catalog

Figure 2(a) shows a portion of the DH type IV catalog, the full version of which is available. 12 Cross-matching with the

LASCO CME catalog provided the properties of the associated CMEs (V_{mean} , acceleration, kinetic energy, mass, and width), forming an additional table shown in Figure 2(b). A description of the catalog, the CME characteristics table, and the DS are available. ¹³ The DH type IV catalog is broadly divided into five sections, namely, type IV properties, type IV source view, quality metrics, CME information, and other info. The first section provides the minimum frequency of emission and the time duration of emission at 14 MHz (referred to hereafter as duration). In cases where multiple spacecraft report on an event, the lowest observed minimum frequency and the longest observed duration are reported in the catalog. This procedure also help us identify the spacecraft that recorded the "best view" of the type IV event. For instance, consider the event in Figure 1(a). The longest duration and the lowest minimum frequency are for the STEREO-A event that subsequently provided the best view of the burst compared to other spacecraft observations. The first section also classifies events into either moving (M) or stationary (S) type IVs across spacecraft while also mentioning the M or S classification in the best-view spacecraft (in "M/S" column). The second section in the table provides details of the multiplevantage-point observations. The spacecraft that recorded the "best view" is noted. Also, all the instruments that detected each event are reported in the "Spacecraft" column. The relative positions of the spacecraft with respect to Earth are provided. Using the CME flare location obtained from the LASCO CME catalog, the relative source locations in the visible solar disk of the STEREO-A, STEREO-B, and Wind spacecraft are estimated for each event. We use

¹² https://cdaw.gsfc.nasa.gov/CME_list/radio/type4/DHtypeIV_catalog.html

¹³ https://cdaw.gsfc.nasa.gov/CME_list/radio/type4

heliographic coordinates, so the source longitude ranges from -90° (east limb) to $+90^{\circ}$ (west limb) across the visible solar disk. Thus, the relative locations of type IV bursts observed by multiple spacecraft provide a database to systematically explore emission directivity over our larger sample. The quality metrics will be introduced in detail in Section 4.1.1. In the CME section of the table, the date, time, flare location, and mean CME speed estimated are provided based on the LASCO CME catalog. The "Other info" section gives information on the solar cycle and the association of DH type II bursts. Combining all this information, we put together a comprehensive DH type IV catalog for the period from 1996 to 2023 May, covering two full solar cycles and the rising phase of cycle 25.

4.1.1. Quality Metrics

The DH type IV catalog reports two quality metrics for each event, namely, "event quality" and "data quality." "Event quality" defines the quality of the detected type IV event along two axes, namely, shape (S) and intensity (I). The events reported by the best-view instrument are ranked based on the dynamic spectral shape and intensity along an integer scale from 1 to 3. Note that 1 is the worst and 3 is the best. The ranking was done based on visual appearance. A type IV burst is expected to appear as a broadband emission with a lowfrequency cutoff. The cutoff can vary with time, and the emission usually lasts for several minutes to hours. Based on how well the above features are traceable in the DS, the shape of the event is ranked. Since the burst morphology is often complicated in the frequency-time plane with multiple variability scales, defining a mathematical model is difficult. Also, in many cases, the event is seen to be confined above 10 MHz, making the shape identification and ranking hard. This is why a manual analysis mode was opted for. Now that we have a manually characterized set, this could be used for building machine learning models for burst identification in the DH band. Figure 3 shows a collage of selected spectra with varying event quality metrics. The square brackets mark the type IV burst emission. Consider the top row in the figure. Moving from I1 to I3, the intensity of the type IV emission can be found to increase with respect to the background, making it easily discernible. However, note that the morphology of the emission is not well defined, and these events are hence identified based on co-observations from other spacecraft and metric-band DS from ground-based telescopes. Direct observation of a postflare loop that brightens up in cotemporal X-ray images was used as supporting evidence, increasing the likelihood of the emission being a type IV, in cases of weak events. Now, consider the rightmost column in the collage. The relative intensity of the emission is very high (I3). As we move from top to bottom, the type IV emission structure can be found to become clearer as the minimum frequency of the emission extends to lower frequencies in the observing window. This effect can be seen moving down the other two columns as well. Note that the middle column shows different moving type IV events. In this scale, the event in the middle panel of Figure 1(a) would be ranked S3I3 due to the distinctive type IV shape and intensity contrast, while the STEREO-B event would be S3I1. However, the catalog would report event quality as S3I3 corresponding to the best detection. The spacecraft with the best quality detection is reported as the "best-view spacecraft" (see Figure 2(a)). We note that events

with a good "S" metric are usually the ones that extend below 10 MHz in the dynamic spectrum and appear relatively isolated in the dynamic spectrum from other bursts, aiding in both detecting and characterizing them better. Often when a type IV burst is not well isolated in the DS, despite its frequency extent or duration, it can get a "shape" metric of 2 rather than 3. A shape metric of 1 could suggest that the event was either in a very crowded part of the DS interlaced with several other bursts or the event did not extend much in the frequency and time axes to discern the shape well.

The "data quality" metric rates the quality of the DS data recorded by all spacecraft during a burst event. The spacecraft are tagged by the letters W, A, and B for Wind, STEREO-A, and STEREO-B, respectively. The metric is formed by combining the letter tag with an integer quality metric. The integer metric is either 0, 1, or 2, denoting the absence of spacecraft data, the existence of poor-quality data, or the availability of good-quality data. Figures 4(a) and (b) show an event where a DH type IV is detected by Wind in the highfrequency channels. Meanwhile, the \sim 2–14 MHz data recorded by STEREO-A are of poor quality to make a robust conclusion. The source was at 63°.9W in the STEREO-A field of view. STEREO-B was nonfunctional during the period. Figure 4(c) shows a simultaneous metric dynamic spectrum showing the event during the same period from an e-Callisto station in Alaska. Meanwhile, the two events shown in Figure 1 are ranked W2A2B2, since the data quality is good in all spacecraft irrespective of the detection of type IVs. The two metrics are crucial for identifying reliable, good-quality observations by multiple spacecraft for a statistical study of the effect of line of sight in the observed radio burst characteristics. However, to explore the mean statistical properties of DH type IV bursts, one can use the values in the type IV properties section, which is by definition based on the "best-view" instrument data.

4.2. Characteristics of DH Type IV Bursts and Associated CMEs

Figure 5(a) shows the histograms of minimum frequency and duration at 14 MHz for all 139 events, while the bottom panel of the figure shows the mean velocity and angular width of the associated CMEs. Note that eight events did not have good LASCO data due to either a data gap or saturation effects from the bright event, which reduced the number of events to 131 in our CME statistics. However, a CME is detected in all eight of these events in the extreme-ultraviolet (EUV) and X-ray images.

Table 1 shows the statistics derived from the property distributions in Figure 5. The median values of duration and minimum frequency are 62 minutes and 7.5 MHz, respectively, while the associated CMEs showed a median $V_{\rm mean}$ of 1223 km s⁻¹, with ~78% (102 out of 131) of them being halo CMEs (e.g., Howard et al. 1982; Zhou et al. 2003; Gopalswamy et al. 2007). Halo CMEs are wide events seen extending around the entire occulting disk of the coronagraph. There is no significant difference in the mean properties of the DH type IV bursts associated with nonhalo CMEs and the larger sample. However, the mean CME speed of nonhalo CMEs causing the DH type IV bursts is around 932 km s⁻¹ compared to the full sample mean of 1301 km s⁻¹. Meanwhile, halo CMEs can be a disk center event, a limb event, or a backside event (Gopalswamy 2004a). However, since the postflare loops and moving plasmoids in backside events will be mostly occulted by

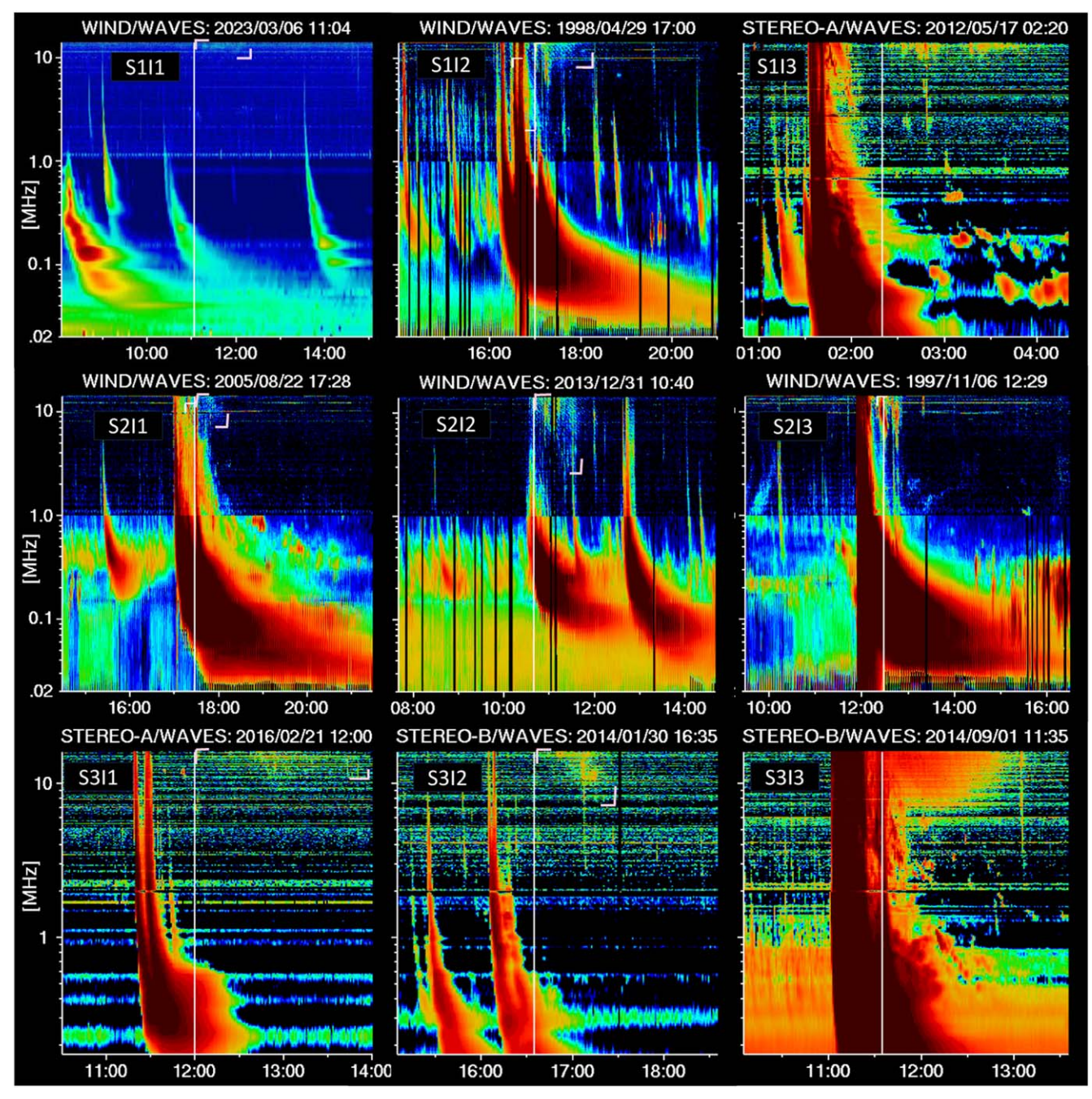


Figure 3. Collage of DH type IV bursts varying in event quality, SiIj, where $i, j \in 1, 2, 3$, with 1 being worst and 3 being best. S refers to the morphology, and I refers to the intensity of the events.

the disk, only the DH type IV bursts associated with frontside or limb events are observable. Figure 6(a) shows the distribution of DH type IV sources on the solar disk as seen by multiple instruments. The dashed lines bound the $\pm 60^{\circ}$ longitude range. About 82% of the sources are concentrated within this region, demonstrating a strong directivity in the longitude distribution of these events. The source latitudes are clearly within $\pm 30^{\circ}$, indicating that the underlying CMEs originate from the active region belt. Only active regions have the ability to produce powerful CMEs that produce DH type IV bursts. The other panels in Figure 6 show the same information on the source distribution, but the marker sizes represent the minimum frequency (b) and the duration of the burst. The sizes are denoted on a scale relative to their respective maximum property

value. The size distribution has no clear dependency on the latitude or longitude of the burst sources.

5. Discussion

The mean CME and radio burst properties listed in Table 1 agree with the previous results by other authors within a few percent (Gopalswamy 2011; Hillaris et al. 2016), except for $V_{\rm mean}$. Gopalswamy (2011) reported a mean $V_{\rm mean}$ of 1526 km s⁻¹, compared to our value of 1301 km s⁻¹. Also, we find a 32% association of DH type IVs with CMEs having $V_{\rm mean} < 1000$ km s⁻¹, as opposed to the 20% (Gopalswamy 2011) and 26% (Hillaris et al. 2016) associations reported earlier. It is possible that our blind search criteria combining

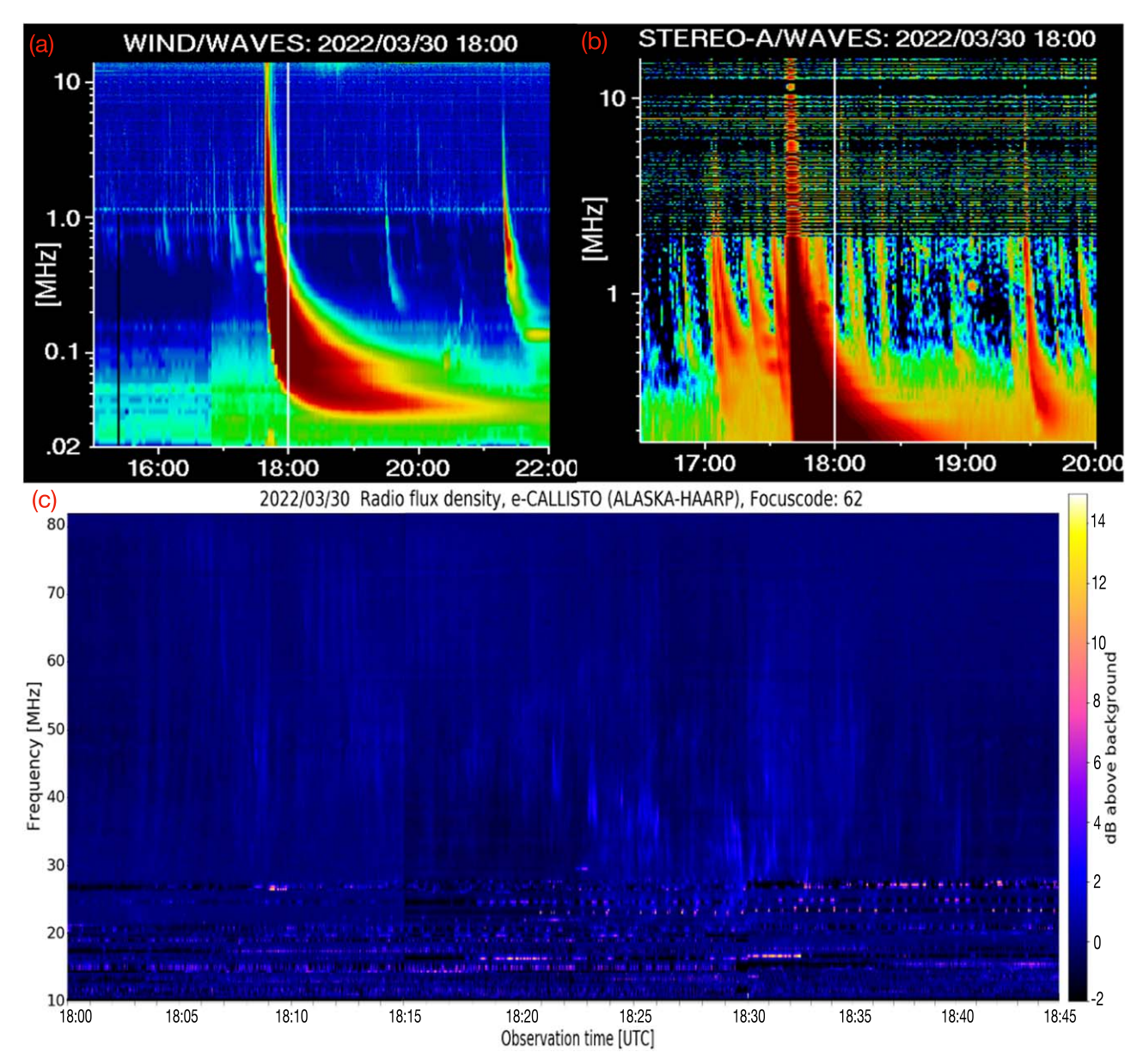


Figure 4. An example event with a data quality metric of W2A1B0. (a) and (b) A DH type IV is clearly detected by Wind/WAVES in >10 MHz between 18:00 and 19:00 UT on 2022 March 30 (W2); the quality of the STEREO-A data in 1–14 MHz is poor (A1), while STEREO-B was nonfunctional during the period (B0). (c) A metric type IV event recorded by an e-Callisto station in Alaska. Data source: http://soleil.i4ds.ch/solarradio/callistoQuicklooks/?date=20220330.

multispacecraft data helped nearly triple the number of DH type IV bursts, with more events associated with weaker CMEs providing a more statistically complete data set. However, we broadly agree with the inferences of the earlier publications that DH type IV bursts typically last for over 1 hr, extend on average to frequencies of ≈7.5 MHz, and are commonly associated with fast (>900 km s⁻¹) and wide (>60°) CMEs. Ninety-six out of 131 bursts (73%) with a well-identified source location have a fast and wide CME association. Also, 78% (102 out of 131) of the bursts are associated with a halo CME. We explored the nonhalo CMEs associated with DH type IV bursts separately. The mean speed and the width of these CMEs also fall well within the definition of a fast and wide CME. Figure 7 shows the solar cycle variation in the DH type IV detection count from the vantage point of the Earth, as seen by Wind/WAVES. The number of type IVs clearly follows the variation in the number of fast and wide CMEs. Though it follows the monthly mean sunspot number,

the correlation is stronger with the number of fast and wide CMEs. This is evident from the fact that the type IV counts even follow the bump around the 2005–2006 period and the dip around 2013 seen in the fast and wide CME counts. However, despite this strong generic association between two, the number of fast and wide CMEs is much higher than that of the DH type IV bursts. In fact, within 1996 November–2023 May, only 18% of the fast halo CMEs produced a DH type IV burst. This means that even if a CME with the most favorable physical attributes occurs in terms of speed and angular extent, the odds of an associated DH type IV burst are fairly low. Besides, DH type IV bursts show a 67% (93 out of 139 events) association with DH type IIs.

5.1. Longitude of Type IV Burst Sources: Emission Directivity

As mentioned earlier, Gopalswamy et al. (2016) showed that the type IV burst sources appear to be concentrated

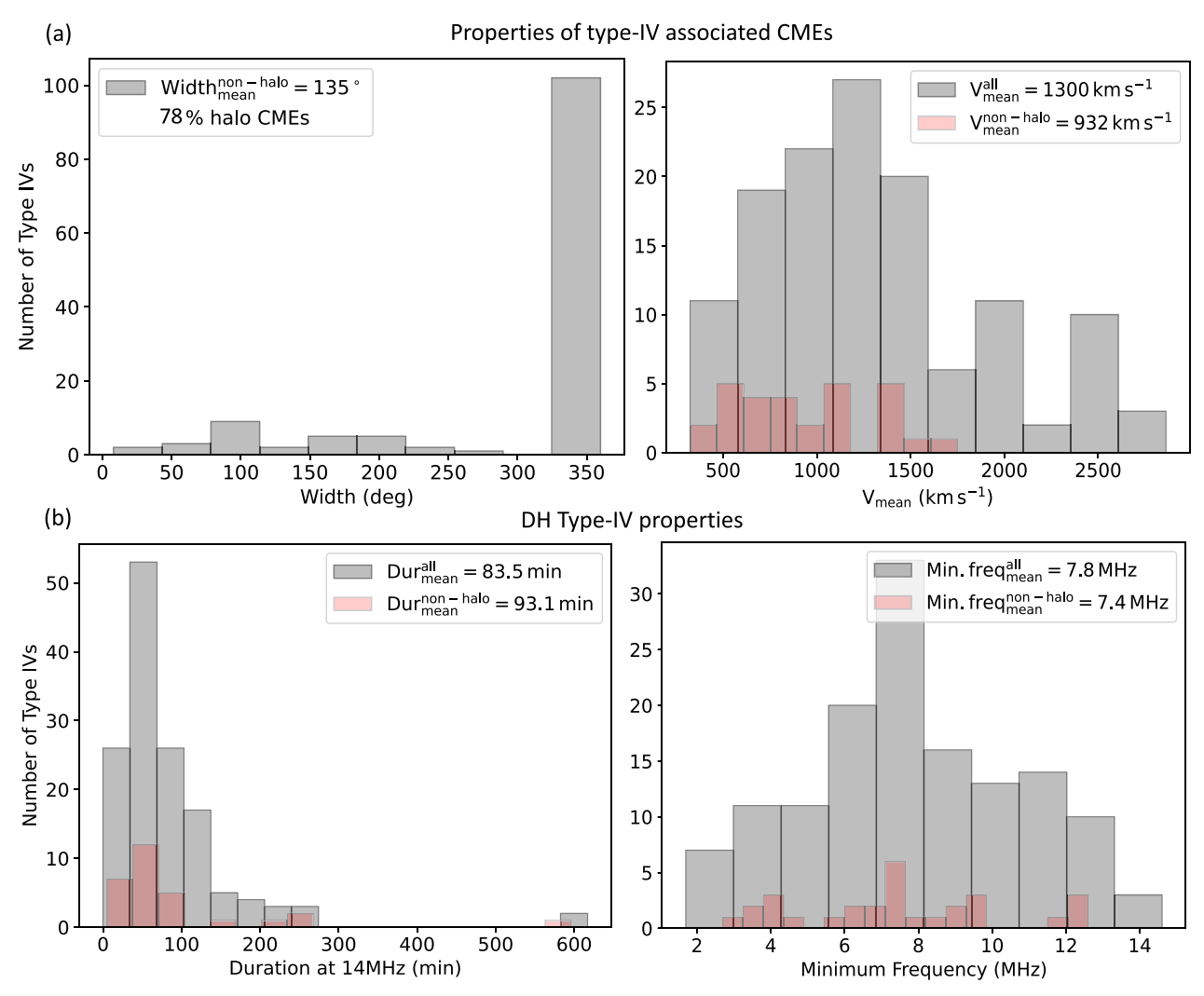


Figure 5. (a) Properties of the CMEs associated with the DH type IV bursts. A total of 78% of the events are halo-CME-associated. (b) Properties of the DH type IV bursts. Legends show the mean values of each property for all bursts and for those associated with nonhalo CMEs. The mean properties of DH type IV bursts caused by nonhalo CMEs are similar to the full sample, but the V_{mean} is slightly lower for the nonhalo events.

Table 1
Statistics of the Various Properties of DH Type IVs and Associated CMEs

	Property	All	Events	Nonhalo CMEs			
	1. 3	Mean	Median	Mean	Median		
DH type IV	Duration (minutes)	83.8	62	93.1	59		
	Min. frequency (MHz)	7.8	7.5	7.4	7.2		
CME	$V_{\rm mean}~({\rm km~s}^{-1})$	1301	1223	932	874		
	Width (deg)	310	360	135	120		

Note. Characteristics of events associated with nonhalo CMEs (width $< 300^{\circ}$) are provided separately. A total of 102 out of 139 events were nonhalo CMEs.

within $\pm 60^{\circ}$ longitude. However, this was based on a type IV burst location distribution derived from cycle 23, a period before the STEREO era. So they also did not have a sample of multiple-vantage-point observations of type IV bursts to verify the directivity in a systematic manner. However, the authors presented a single case study of an event from 2013 November 7 that was observed with the Wind and STEREO spacecraft. The DH type IV event was found to be best observed by the

spacecraft that was viewing the event within $\pm 60^{\circ}$. Based on this, the authors argued that there could be a directivity in the inherent emissivity, besides any effect due to background plasma opacity. A few case studies that followed this paper argued that occultation by dense overlying material, often a CME streamer shock formed toward the CME flank region, could be a prime reason for blocking the emission along certain viewing angles and not necessarily inherent emissivity (Melnik et al. 2018; Talebpour Sheshvan & Pohjolainen 2018; Pohjolainen & Talebpour Sheshvan 2020). Thus, the earlier studies that explored directivity in the emission have either been on specific cases or on the distribution of observed source locations from one spacecraft without factoring in the variation in the dynamic spectral morphology detected from multiple vantage points. The DH type IV catalog presented here has event and data quality metrics that grade the characteristic detail in the observed DS of each DH type IV event for each spacecraft located at different vantage points. Based on these metrics, the catalog also mentions the best-view spacecraft that detected the type IV burst with the best extent in frequency and time of all recorded data from multiple viewpoints. This let us

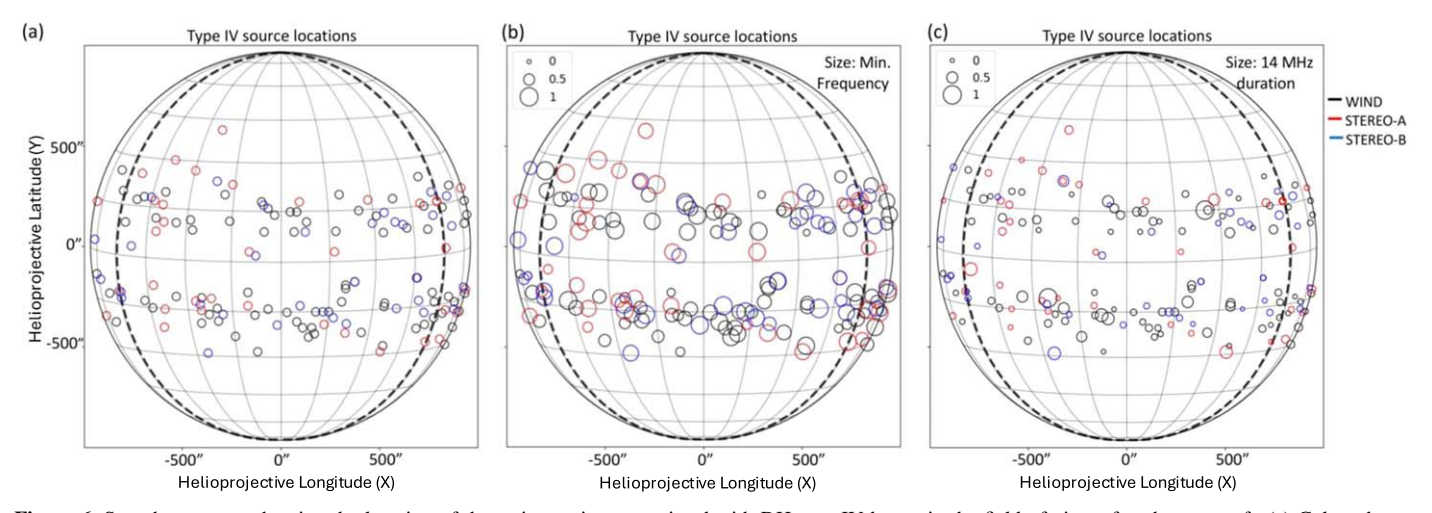


Figure 6. Stonyhurst maps showing the location of the active regions associated with DH type IV bursts in the field of view of each spacecraft. (a) Colors denote different spacecraft. A total of 82% of the type IV sources lie within $\pm 60^{\circ}$ longitude, demarcated by the dashed lines. The source latitudes, except in one case, are confined within $\pm 30^{\circ}$. (b) and (c) Same information as (a), with the marker size denoting the minimum frequency and the duration of the burst on a scale relative to the respective maximum value. Neither minimum frequency nor duration show a clear preference to source location.

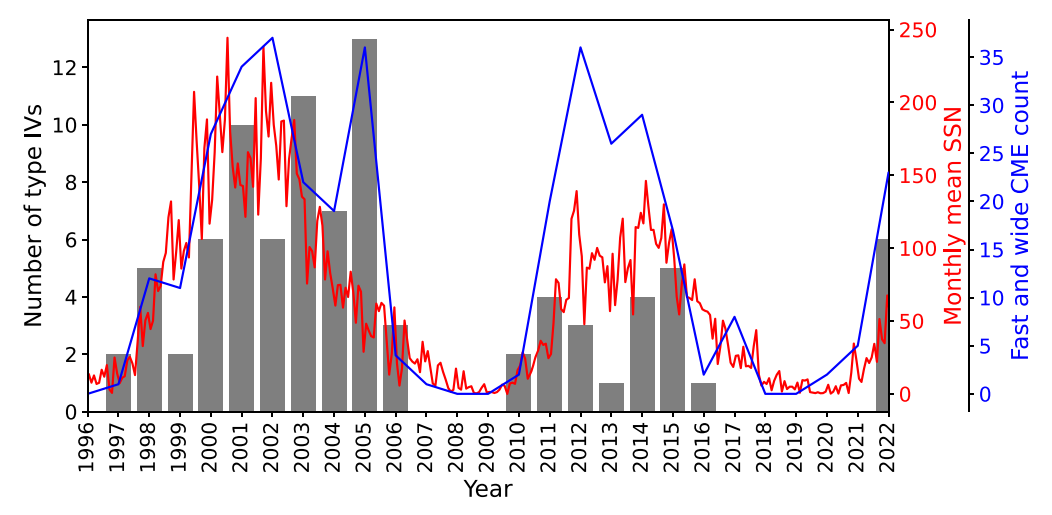


Figure 7. Solar cycle variation in the number of DH type IV bursts observed by Wind/WAVES. Monthly mean sunspot number (red) and the number of fast and wide CMEs (blue) are shown. A total of 73% of the DH type IV bursts in the catalog are associated with a fast and wide CME.

study the direction dependency in not only the detection of the DH type IV burst but also its morphological details in the DS.

To systematically explore the effects of viewing angle, the bursts detected with a good event quality of SiIj, where i, $j \in \{2, 3\}$, were first chosen. From these events, only those that occurred when at least two spacecraft were producing good DS with a data quality of 2 were chosen. This produced a subset of 48 events with good multiple-vantage-point observations of the Sun from at least two viewpoints. The list of events with burst and CME characteristics and assigned event IDs is available.¹⁴ The event ID simply tags each event. Figure 8 shows the expected source longitudes of the selected DH type IV burst sources (i.e., flare loops) in the frame of each spacecraft. Locations of the best-observed burst events are marked by colored circles, other detected source longitudes by triangles, and nondetections by squares. The nondetection longitudes provide the source location of the associated flare in the reference frame of the spacecraft that failed to detect it. Marker

colors of the best-viewed detections denote $V_{\rm mean}$, and sizes denote the type IV duration. Figure 9 is similar to Figure 8, with the exception that the sizes denote minimum frequency. First, the role of viewing angle (or apparent source longitude) in the detection of DH type IV bursts is explored. We find that 58 out of 62 observations (94%) made within $\pm 60^{\circ}$ source longitude by various spacecraft detected a burst (see circles and triangles). Meanwhile, only 9 out of 20 observations (45%) made between $\pm 60^{\circ}$ and $\pm 105^{\circ}$ were detections. Of the total type IV detections reported when the spacecraft are viewing the source at an angle within $\pm 105^{\circ}$, only 13% (9 out of 67) are contributed by spacecraft viewpoints >|60°|. An upper limit of 105° is set on the source longitude because of a few type IV detections associated with flares that occurred slightly behind the limb. The postflare loops or plasmoids that caused the radio burst in these events extended sufficiently beyond the limb, making them visible, as evidenced by the associated EUV movies. For instance, event 47 was detected by two spacecraft, both viewing it close to the limb with flare source longitudes of 85° and 105°. Figure 10 shows the DS for the event along with EUV and white-light coronagraph images from the two

¹⁴ https://cdaw.gsfc.nasa.gov/CME_list/radio/type4/All_good_multiview_events.html

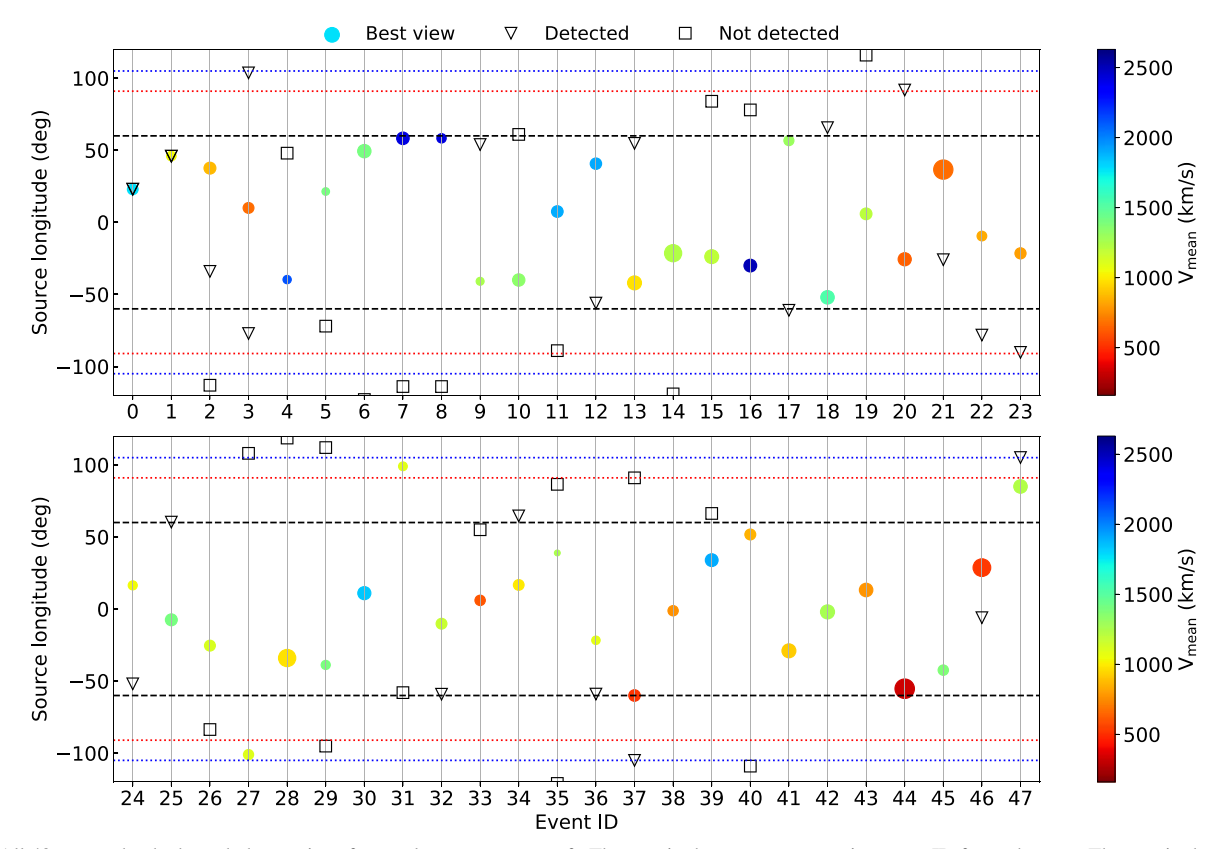


Figure 8. All 48 events that had good observations from at least two spacecraft. The X-axis shows a representative event ID for each event. The Y-axis shows the burst source longitude relative to the spacecraft vantage point. The relative source longitudes that gave a detection are marked by triangles and circles, with circles marking the best detection. The sizes of the circles represent the burst duration, while the colors denote V_{mean} . Dashed horizontal lines mark $\pm 60^{\circ}$, $\pm 90^{\circ}$, and $\pm 105^{\circ}$ longitudes. Longitude >|90| represents flare sources behind the limb. In some cases where the postflare loop rose much higher, a type IV emission could be detected from flare sources slightly behind the limb.

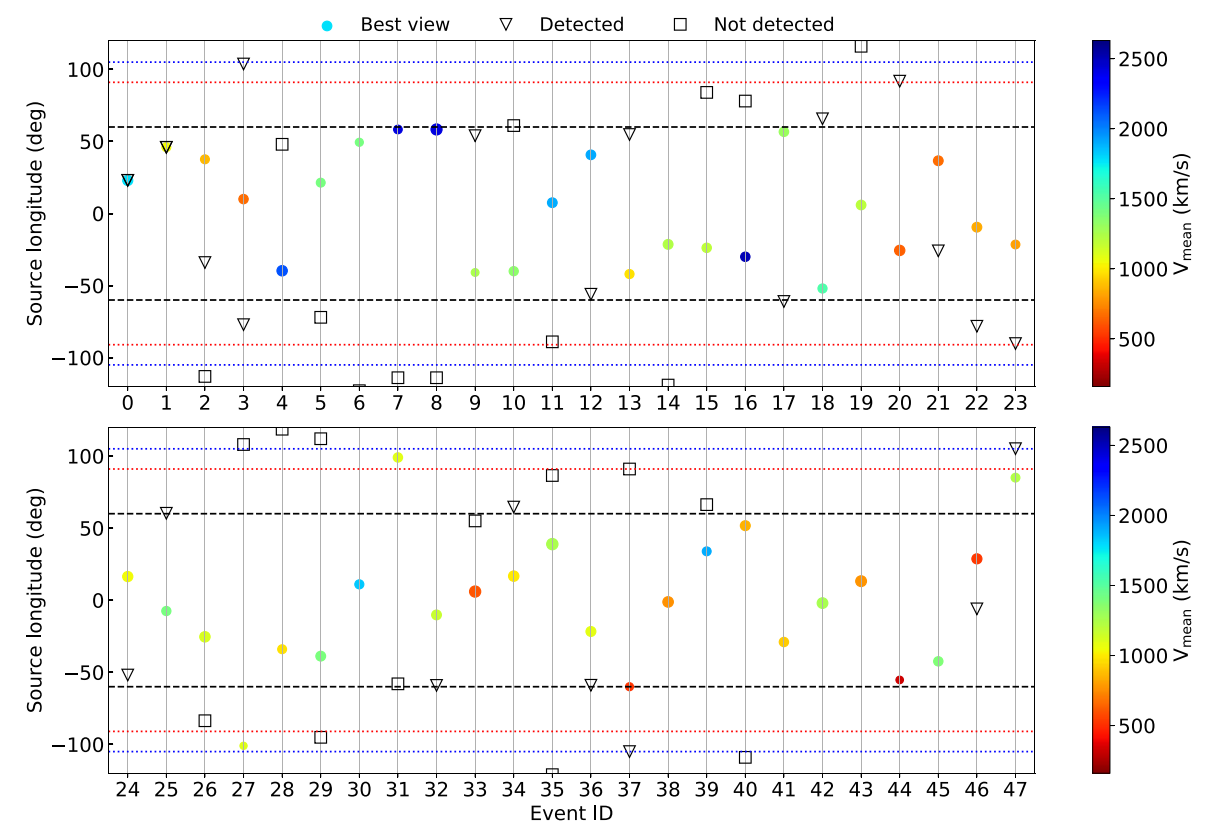


Figure 9. Same as Figure 8. The sizes of the circles represent minimum frequency.

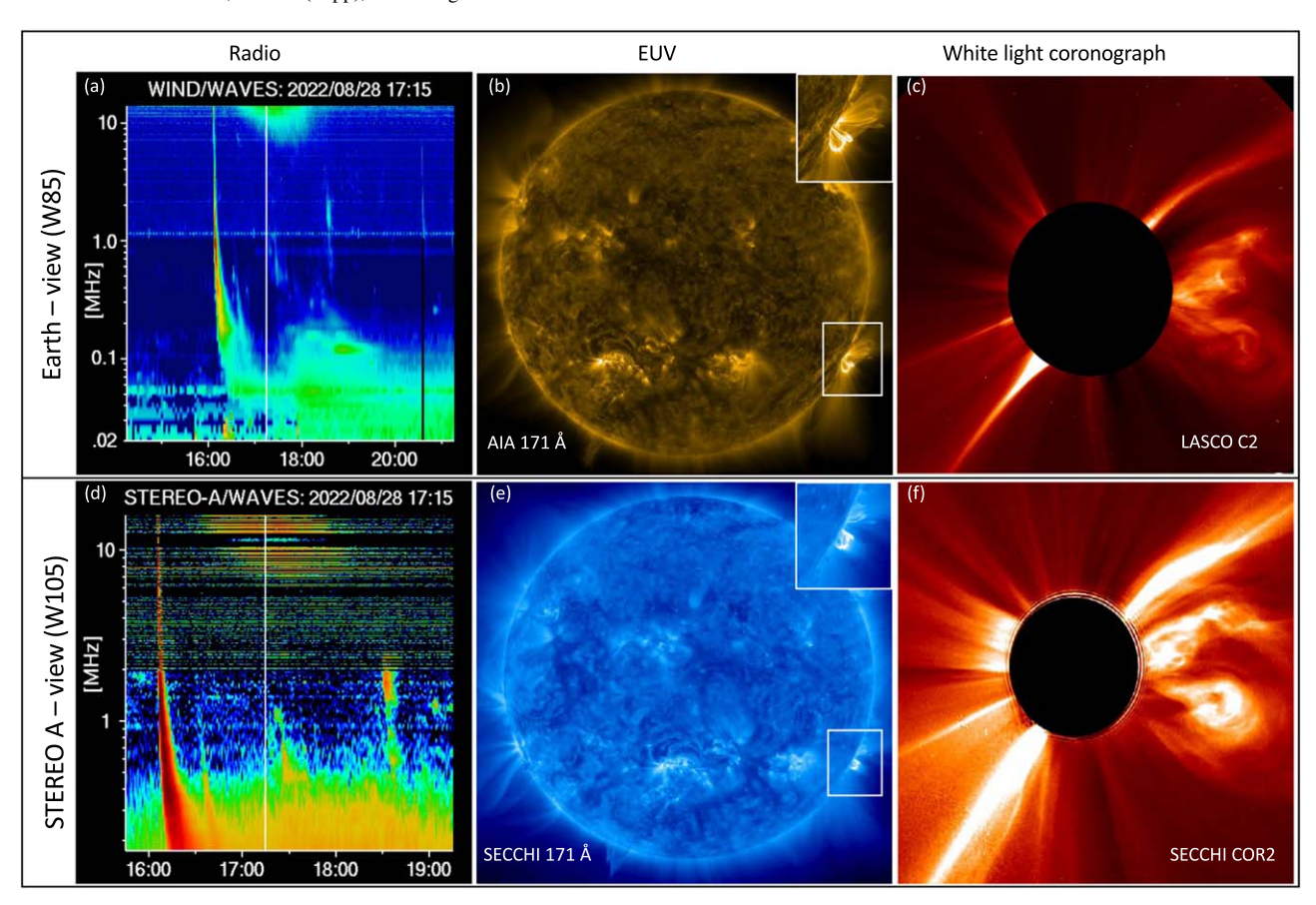


Figure 10. Case of a type IV from a flare source behind the limb (event 47): radio, EUV, and white-light coronagraph observations of a limb CME event from the viewpoints of the Earth (top row) and STEREO-A (bottom row). Source locations are specified on the left of each row (Wind: 85°W; STEREO-A: 105°W). STEREO-A was at 20°E with respect to the Earth. A DH type IV burst was observed by both spacecraft. An associated postflare loop is visible over the limb in the EUV maps from both vantage points. The insets in the middle panel zoom in to the loop region. The rightmost panels show the CME in the coronagraphs from the Earth and STEREO-A vantage points.

spacecraft that detected it. The EUV and coronagraph images correspond to the time instants marked by the lines in the DS. A postflare loop can be found rising beyond the limb in the EUV images. This implies that the DH type IV bursts are detectable even beyond the limb (>90° source longitude), provided the postflare loop is visible over the limb and there are no dense occulting structures along the line of sight. From Figure 8, only three detections are reported out of the 14 such observations from a $\gtrsim\!\!90^\circ$ source line of sight.

Now we explore the effect of viewing angle in the observed morphology in the radio DS. From Figure 8, it can be seen that for every event, the spacecraft that recorded the best view (marked by circles) was always within $\pm 60^{\circ}$ longitude, provided there was a spacecraft observing the source within that range. The only exception to this rule is event 31, which was hence studied in detail. Figure 11 shows the observations of the event in radio, EUV, and white-light coronagraph as seen from the viewpoints of the Earth (top row) and STEREO-B (bottom row). A DH type IV burst was detected by STEREO-B but not by Wind, despite the latter viewing the source at $\sim 60^{\circ}$. Meanwhile, for STEREO-B, this was a limb event. The postflare loop is clearly visible at the limb from the STEREO-B viewpoint as seen in the 171 Å image from the SECCHI instrument on board STEREO-B. The inset of Figure 11(e) shows a zoomed-in image of the region. However, the 171 Å image of the flaring region as seen from Earth, taken by the

Atmospheric Imaging Assembly on board the Solar Dynamics Observatory, reveals a complex active region configuration (Figure 11(b)). The insets in the panel zoom into the flaring active region in the 171 Å (top right) and HMI continuum (bottom right) maps. The HMI map reveals a complex $\beta\gamma$ sunspot group near the flare site. Also, another active region can be spotted (marked by an arrow) within 10° separation of the one in question. Hence, given the complex magnetic field configuration in the neighborhood of the flare site, the radio bursts are likely occulted by the dense plasma in the complex posteruption field structures. The effect of source occultation on type IV burst detection has been discussed in earlier works (e.g., Talebpour Sheshvan & Pohjolainen 2018; Pohjolainen & Talebpour Sheshvan 2020). This occultation effect could also be the cause of the disruption of the type I noise storm in the Wind DS after \approx 16:20 UT, when the CMEassociated type III burst occurred. Meanwhile, the type IV burst recorded by STEREO-B is a moving type IV and starts around 16:50 UT, when the plasmoid structure marked by a white arrow in Figure 11(f) first appears in the SECCHI COR2 field of view.

The inferences from the overall statistics and the special case of event 31 suggest that in the absence of dense structures along the line of sight that can occult the view, a DH type IV burst is best viewed when the spacecraft is within the $\pm 60^{\circ}$ line of sight. However, DH type IV bursts can be detected

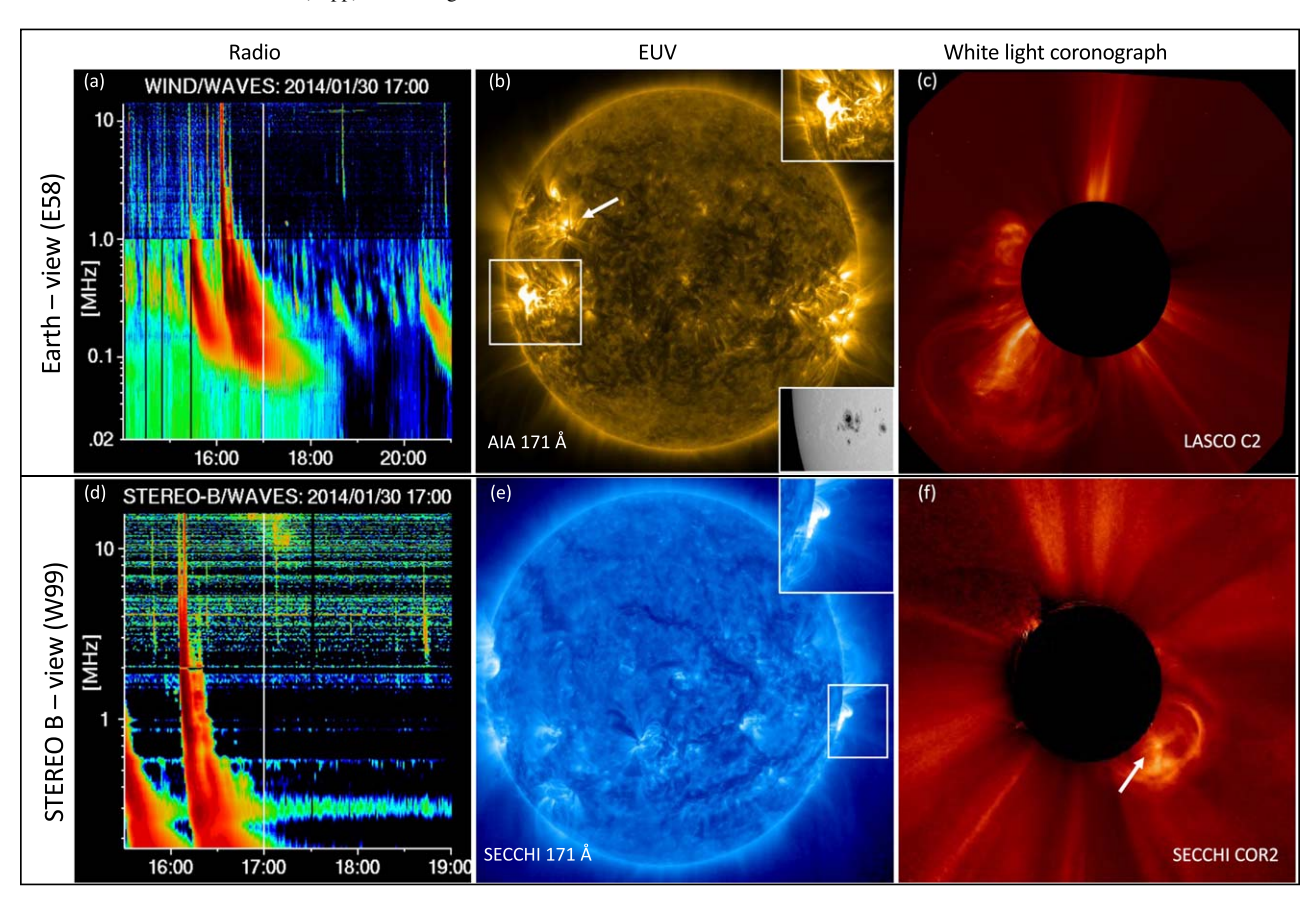


Figure 11. Case of event 31: radio, EUV, and white-light coronagraph observations of the CME from the viewpoints of the Earth (top row; source longitude: 58°E) and STEREO-B (bottom row; source longitude: 99°W). STEREO-A was at 150°W with respect to the CME source. A DH type IV burst is detected by STEREO-B but not Wind. Insets in the top right region of panels (b) and (e) zoom in to the white boxes that mark the flaring region. In panel (b), an HMI image of the flaring region is provided in the bottom right inset. The arrow in panel (b) marks the nearby active region, while in panel (f), the arrow points at the CME plasmoid temporally correlated with the observed DH type IV. The active region marked in panel (b) is the likely source of the noise storm in Wind/WAVES in the preflare period (before ~16:00 UT). STEREO-B does not detect this emission, possibly because of the directivity weakening the flux density of the noise storm source, which is only partly visible at the limb in the STEREO-B field of view.

even from limb sources when there is no significant line-of-sight occultation (e.g., event 47), though this need not be the line of sight that provides the best view of the event. This is as expected from the hypothesis of Gopalswamy et al. (2016) that the type IV emission could have inherent directivity in the emission, making it best viewed within the $\pm 60^{\circ}$ line of sight out of all possible detections in different lines of sight.

5.2. Relations between DH Type IV Properties, Associated CME, and Viewing Angle

Since the viewing angle or, equivalently, the observed source longitude is a crucial factor in obtaining the best view of the burst, it is possible that the properties of the radio burst in the DS might depend on source longitude. But the colors and sizes of the circles in Figures 8 and 9 do not show any particular pattern in their distribution across the longitude axis. Since the colors denote $V_{\rm mean}$, this means that the CME speed is not a crucial determinant in deciding the detectability of a type IV burst even close to the limb. Similarly, the duration (in Figure 8) and minimum frequency (in Figure 8) of the radio burst denoted by the sizes also do not show any definitive trend across the longitude axis. This means that the emission directivity may not have a major impact on the

observed DS characteristics. We further explored the patterns and interrelations, if any, in the multiparameter space of the properties of the observed type IV burst, associated CME, and viewing angle. Only events with event quality SiIj such that i, $j \in 2$, 3 were chosen for this study. Figure 12 shows the variation in $V_{\rm mean}$, type IV duration, minimum frequency, and best-view source longitude for all selected events. We use the absolute value of the source longitudes since the effect of viewing angle should be symmetric about the central meridian. Different panels explore the event characteristics for halo, nonhalo, and fast and wide CME-associated events. Halo and nonhalo CMEs were separately studied because the CME width histogram in Figure 5(b) shows a bimodal distribution. Also, the fast and wide CMEs were explored separately, since their occurrence rates are seen to correlate well with those of DH type IV counts (see Figure 7). The detection of DH type IV bursts with durations longer than 120 minutes (horizontal black line) seems to prefer a source longitude within $\pm 60^{\circ}$. A more detailed clustering analysis is currently underway by expanding the CME property table (Figure 2(b)) with more physical characteristics of the CME and associated flare. This is beyond the scope of this paper, which is aimed at presenting the catalog, statistics, type IV directivity, and preliminary inferences on clustering of various properties of these events.

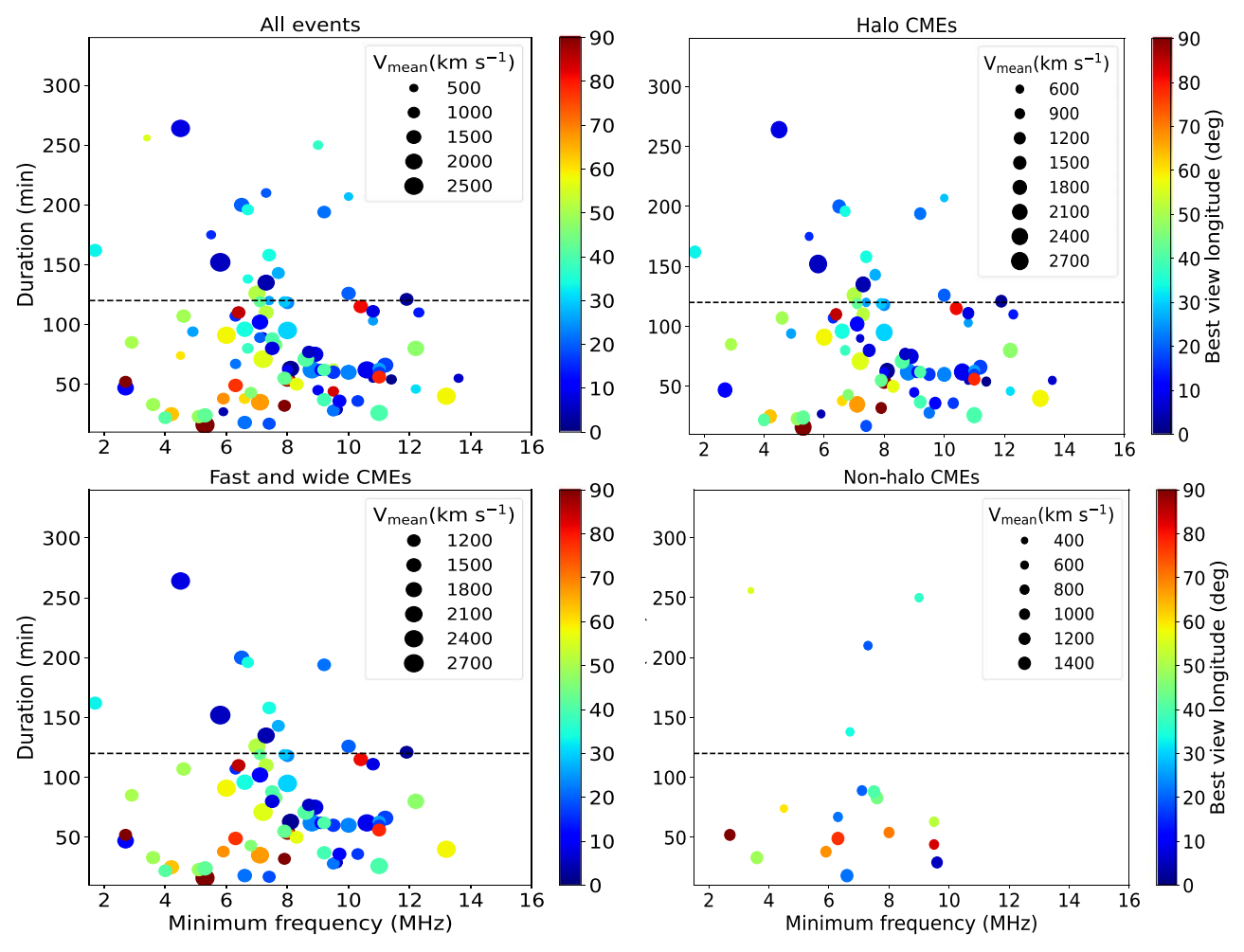


Figure 12. Properties of DH type IV events with quality of at least Silj, where $i, j \in 2$, 3. The modulus of the source longitude is shown in color scale, while sizes denote V_{mean} . The horizontal line marks 120 minutes.

6. Conclusion

We present a comprehensive catalog of DH type IV bursts during the period between 1996 November and 2023 May, covering two complete solar cycles (23 and 24) and the rising phase of the current cycle. The catalog is complete to the entire LASCO CME event list and also covers the period of reported metric type IV and DH type II bursts. All DH type IV bursts are associated with white-light CMEs, in contrast to the case of metric type IV bursts. Also, we include radio data gathered by three spacecraft, namely, Wind, STEREO-A, and STEREO-B. This not only helps increase the source count but also provides multiple-vantage-point observations for several DH type IV bursts, letting us explore the intriguing aspect of emission directivity. The final catalog has 139 DH type IV bursts, along with the properties of the associated CMEs. Since the DH-band dynamic spectrum is a disk-integrated observable, the presented catalog forms a Sun-as-a-star database to explore the CME-related type IV bursts, which are one of the muchsought-after radio signatures of stellar CMEs.

DH type IV bursts are mostly associated with halo CMEs (78%; 102 out of 131 events) with a mean speed of 1301 km s⁻¹. Ninety-three out of 139 events had a DH type II association. The solar source longitudes of the detected events lie within $\pm 60^{\circ}$ for 58 out of 62 cases where multiple spacecraft observed the same source from different vantage

points. The source latitudes of all except one type IV source are found to be within $\pm 30^{\circ}$ latitude, pointing at the association of a strong CME causing active regions with DH type IV bursts. The sole outlier is, however, within $\pm 45^{\circ}$. Our statistical results over a sample thrice larger than previous studies confirm the earlier results by different authors (e.g., Gopalswamy 2011; Gopalswamy et al. 2016) in a statistically robust manner. We find a strong correlation between the occurrence of these bursts with that of the fast and wide CMEs during the catalog period. However only 18% of the fast halo CMEs that occurred during the catalog period produced a DH type IV burst. So a DH type IV detection indicates a high likelihood for the occurrence of a fast halo CME, but the converse is not true.

Using the multiple-vantage-point observation data from the Wind and STEREO spacecraft, the effect of directivity on the detection of these bursts and their observed morphology in DS was explored. When 94% of cases where the spacecraft was observing a flare source within the $\pm 60^{\circ}$ line of sight ended up in a detection, only 45% of the observations made outside this field of view reported a burst. In cases where multiple spacecraft observed an event, it is found that the spacecraft that observed the burst source within $\pm 60^{\circ}$ longitude recorded the burst with the longest duration and extending down to the lowest frequency in the DS, thereby providing the best or most detailed view of the event. This rule had only one exception in the entire catalog,

in which case we find evidence for significant occultation of radio emission by surrounding magnetic field structures. However, in the absence of significant line-of-sight occultation, type IV bursts from even limb events can be detected, though these detections may not provide the best possible view of the event. Additionally, the detection of a burst with a duration >120 minutes strongly prefers a viewing angle within $\pm 60^{\circ}$. Based on these results, we infer that, though detecting a DH type IV is possible at source longitudes extending up to the limb, a comparison of the DS for the same burst as seen by multiplevantage-point missions does suggest an inherent directivity in the radio emission that prefers $a \pm 60^{\circ}$ viewing cone as hypothesized by Gopalswamy et al. (2016).

Acknowledgments

We thank the CDAW team for maintaining an up-to-date catalog of LASCO/CME events and processed dynamic spectra from the Wind and STEREO spacecraft. We also thank SWPC, Radio Monitoring, Australian Space Weather Data Center, and e-Callisto network for the open-access database they maintain for various solar events. A.M. acknowledges the discussions with the Sunpy team via the Elements¹⁵ platform. A.K.'s research was supported by an appointment to the NASA Postdoctoral Program at the NASA Goddard Space Flight Center (GSFC). A.M. and N.G. are supported in part by NASA's STEREO project and LWS program. S.A. was partially supported by NSF grant AGS-2043131. S.G.'s research was supported by NSF grant AGS-22289. A.M. acknowledges the developers of the various Python modules, namely, Numpy (Harris et al. 2020), Astropy (Astropy Collaboration et al. 2013), Matplotlib (Hunter 2007), and multiprocessing. A.M. also thanks the developers of CASA (McMullin et al. 2007). A.M. acknowledges the help from Seiji Yashiro in posting the catalog online and for maintaining the various CDAW data resources. A.M. acknowledges Pertti Mäkelä for useful discussions and sharing of data.

Facilities: Wind (WAVES), STEREO (SWAVES), SOHO (LASCO), SDO (AIA).

Software: Numpy (Harris et al. 2020), Astropy (Astropy Collaboration et al. 2013), Matplotlib (Hunter 2007), Multiprocessing (McKerns et al. 2012), Pandas (The pandas development team 2020), Urllib, ¹⁶ Beautifulsoup, ¹⁷ Sunpy (The SunPy Community et al. 2020), Datetime, ¹⁸ Scipy (Virtanen et al. 2020), Helioviewer (Ireland et al. 2009).

ORCID iDs

Atul Mohan https://orcid.org/0000-0002-1571-7931 Nat Gopalswamy https://orcid.org/0000-0001-5894-9954 Anshu Kumari https://orcid.org/0000-0001-5742-9033 Sachiko Akiyama https://orcid.org/0000-0002-7281-1166 Sindhuja G https://orcid.org/0000-0002-5893-1938

References

Astropy Collaboration, Robitaille, T. P., & Tollerud, E. J. 2013, A&A, 558, A33

Boischot, A. 1957, CRAS, 244, 1326

```
Mohan et al.
Boischot, A., & Clavelier, B. 1968, in IAU Symp. 35, Structure and
   Development of Solar Active Regions, ed. K. O. Kiepenheuer (Dordrecht:
   D. Reidel), 565
Bougeret, J. L., Kaiser, M. L., Kellogg, P. J., et al. 1995, SSRv, 71, 231
Brueckner, G. E., Howard, R. A., Koomen, M. J., et al. 1995, SoPh, 162,
Cane, H. V., & Reames, D. V. 1988a, ApJ, 325, 901
Cane, H. V., & Reames, D. V. 1988b, ApJ, 325, 895
D'Huys, E., Seaton, D. B., Poedts, S., & Berghmans, D. 2014, ApJ, 795, 49
Dulk, G. A., & Altschuler, M. D. 1971, SoPh, 20, 438
Duncan, R. A. 1981, SoPh, 73, 191
Gopalswamy, N. 2004a, in A Global Picture of CMEs in the Inner Heliosphere,
   ed. G. Poletto & S. T. Suess (Dordrecht: Springer Netherlands), 201
Gopalswamy, N. 2004b, in Solar and Space Weather Radiophysics,
   Astrophysics and Space Science Library, ed. D. E. Gary & C. U. Keller,
   Vol. 314 (Dordrecht: Springer), 305
Gopalswamy, N. 2011, in Planetary Radio Emissions VII (PRE VII), Proc. 7th
   International Workshop, ed. H. O. Rucker et al. (Vienna: Austrian Academy
   of Sciences Press), 325
Gopalswamy, N., Aguilar-Rodriguez, E., Yashiro, S., et al. 2005, JGRA, 110,
Gopalswamy, N., Akiyama, S., Mäkelä, P., Yashiro, S., & Cairns, I. H. 2016,
   arXiv:1605.02223
Gopalswamy, N., & Kundu, M. R. 1989, SoPh, 122, 145
Gopalswamy, N., Mäkelä, P., & Yashiro, S. 2019, SunGe, 14, 111
Gopalswamy, N., Yashiro, S., & Akiyama, S. 2007, JGRA, 112, A06112
Gopalswamy, N., Yashiro, S., Michalek, G., et al. 2009, EM&P, 104, 295
Hansen, R., Garcia, C., Grognard, R.-M., & Sheridan, K. 1971, PASA, 2,
Harris, C. R., Millman, K. J., van der Walt, S. J., et al. 2020, Natur, 585,
  357
Hillaris, A., Bouratzis, C., & Nindos, A. 2016, SoPh, 291, 2049
Howard, R. A., Michels, D. J., Sheeley, N. R. J., & Koomen, M. J. 1982, ApJL,
   263, L101
Howard, R. A., Moses, J. D., Vourlidas, A., et al. 2008, SSRv, 136, 67
Hunter, J. D. 2007, CSE, 9, 90
Ireland, J., Hughitt, K., Müller, D., et al. 2009, AAS/SPD Meeting, 40, 15.01
Kumari, A., Morosan, D. E., & Kilpua, E. K. J. 2021, ApJ, 906, 79
Kumari, A., Morosan, D. E., Kilpua, E. K. J., & Daei, F. 2023, A&A,
   675, A102
Kundu, M. R., & Spencer, C. L. 1963, ApJ, 137, 572
McKerns, M. M., Strand, L., Sullivan, T., Fang, A., & Aivazis, M. A. G. 2012,
   arXiv:1202.1056
McLean, D., & Labrum, N. 1985, Solar Radio Astrophysics (Cambridge:
   Cambridge Univ. Press)
McMullin, J. P., Waters, B., Schiebel, D., Young, W., & Golap, K. 2007, in
   ASP Conf. Ser. 376, Astronomical Data Analysis Software and Systems
   XVI, ed. R. A. Shaw, F. Hill, & D. J. Bell (San Francisco, CA: ASP),
Melnik, V. N., Brazhenko, A. I., Konovalenko, A. A., et al. 2018, SoPh,
   293, 53
Miteva, R., Samwel, S. W., & Krupar, V. 2017, JSWSC, 7, A37
Mohan, A., Mondal, S., Wedemeyer, S., & Gopalswamy, N. 2024, A&A,
   686, A51
Morosan, D. E., Kumari, A., Kilpua, E. K. J., & Hamini, A. 2021, A&A,
Patel, B. D., Joshi, B., Cho, K.-S., & Kim, R.-S. 2021, SoPh, 296, 142
Pohjolainen, S., & Talebpour Sheshvan, N. 2020, AdSpR, 65, 1663
Robbrecht, E., Patsourakos, S., & Vourlidas, A. 2009, ApJ, 701, 283
Robinson, R. D. 1978, SoPh, 60, 383
Schmahl, E. J. 1972, PASA, 2, 95
Smerd, S. F. 1970, PASA, 1, 305
Smerd, S. F. 1971, AuJPh, 24, 229
Takakura, T. 1961, PASJ, 13, 166
Takakura, T., & Kai, K. 1961, PASJ, 13, 94
Talebpour Sheshvan, N., & Pohjolainen, S. 2018, SoPh, 293, 148
The pandas development team 2020, pandas-dev/pandas: Pandas, v2.2.2,
   Zenodo, doi:10.5281/zenodo.10957263
The SunPy Community, Barnes, W. T., Bobra, M. G., et al. 2020, ApJ, 890, 68
Virtanen, P., Gommers, R., Oliphant, T. E., et al. 2020, NatMe, 17, 261
Weiss, A. A. 1963, AuJPh, 16, 526
Wild, J. P. 1970, PASAu, 1, 365
Yashiro, S., Gopalswamy, N., Michalek, G., et al. 2004, JGRA, 109, A07105
Young, C. W., Spencer, C. L., Moreton, G. E., & Roberts, J. A. 1961, ApJ,
```

133, 243

Zhou, G., Wang, J., & Cao, Z. 2003, A&A, 397, 1057

Zic, A., Murphy, T., Lynch, C., et al. 2020, ApJ, 905, 23

¹⁵ https://app.element.io/#/room/#sunpy:openastronomy.org

¹⁶ https://docs.python.org/3/library/urllib.html

https://www.crummy.com/software/BeautifulSoup/bs4/doc/

¹⁸ https://pypi.org/project/DateTime/